Modelling, simulation and design of a testable 200 W$_e$ dual generator free-piston Stirling engine

B.J.G. de la Bat [a, *], R.T. Dobson[b]

[a] University of Stellenbosch, Department of Mechanical and Mechatronic Engineering, Private Bag X1, Matieland 7602, South Africa, 16606914@sun.ac.za
[b]RTD@sun.ac.za

*Corresponding author: 16606914@sun.ac.za

Topic/s: Simulation, design, development, testing, free-piston, Stirling engine

Keywords: free-piston, Stirling engine, dual piston, modelling, design, development, testing

ABSTRACT

A free-piston Stirling engine (FPSE) electric generator is a type of Stirling engine in which the displacer and piston are not linked via a kinematic mechanism, such as a crankshaft, as in conventional kinematic Stirling engines. The displacer and piston run mechanically free of one another in a shared natural frequency, driven only by an internal oscillatory pressure wave. The engine is essentially frictionless and does not require lubrication, thereby greatly enhancing the lifetime of the engine. A FPSE utilises a linear electric generator as opposed to the conventional rotary generator. The entire engine is hermetically sealed and requires no servicing during the engine lifetime, this being but one of the advantages of FPSEs over kinematic Stirling engines.

This paper presents the modelling and design of a FPSE prototype that is currently being developed. Theoretical modelling was accomplished by discretising the working space into a network of finite one-dimensional control volumes. The conservation of mass, momentum and energy was applied to each control volume and in so doing a system of finite difference equations was generated. A Fortran 95 computer simulation program was developed to solve the governing system equations by using a fully-explicit method. The development of a prototype engine is discussed which is partially based on the design by Microgen Corporation, but with the addition of a secondary generator attached to the displacer. Design considerations of the prototype were based on the insights gained from simulating the operation of the engine.

1. INTRODUCTION

The term free-piston Stirling engine (FPSE) refers to a type of Stirling engine where the piston and displacer are not linked by a crankshaft mechanism, distinguishing the FPSE from conventional kinematic Stirling engines. This modification to Stirling's original engine is often credited to Professor William Beale from Ohio University [1]. The power piston is essentially "free" of mechanical linkage and its motion is only dependant on the load and working fluid pressure forces acting inside the engine. The piston and displacer are driven in a shared natural frequency by an oscillatory pressure wave that exists because of the cyclic heating and cooling of the working fluid.

Because the FPSE does not have a revolving crankshaft, the engine is essentially frictionless and does not require lubrication. The entire engine is sealed hermetically and requires no servicing during its lifetime. Flexure springs attached to the respective displacer and piston cyclically store and release mechanical energy, which is equivalent to the angular momentum stored in the flywheel of a conventional engine. Power is usually extracted from the engine by means of a linear electric generator that is attached to the power piston, although the piston can also be used to deliver hydraulic power in a hydraulic free-piston Stirling engine configuration.

Stirling engines are also known for high thermal-to-electric efficiencies and versatility as external combustion engines. Heating can be supplied by almost any heat source with well-known examples including heating by radioisotope energy, waste incineration, open flame combustion and concentrated solar power [2]. When combined with parabolic dish concentrator systems, they are capable of supplying both usable electric power and hot water as co-generation systems. This identifies such an engine as a strong candidate for combined heat and power (CHP) delivery in a so-called "smart grid" layout, where energy resources are shared in an off-grid community [3]. Because many parts of South Africa and Africa remain to a large extent rural to this day, the FPSE has been selected as a plausible solution to provide both heat and power to isolated communities.

The University of Stellenbosch has conducted a number of studies on FPSEs and has recently attained a Trinum co-generation dish Stirling engine from Innova, Italy [4]. Most recently Deetlefs [5] modelled the working principle based on the Beale B-10B demonstrator engine from Sunpower Incorporated with an attached electric generator, however the generator was not well matched for the engine. Deetlefs recommends that a weak electric generator must be developed for a prototype so as to keep the generator magnet train from locking with the generator core under low temperature conditions. An outcome of the studies is that in order to generate usable power under varying load conditions, the displacer and piston motions need to be controlled. A testable and modular prototype that is based partially on the geometry of the Microgen Corporation [6] type and that of the Twinbird free-piston cryocooler [7], in which a displacer rod runs through the centre of the power-piston, is under development. A secondary and smaller generator, known as the mover, is attached to the displacer rod to allow for direct displacer control, as suggested by Strauss [8]. The mover can also be used to start the engine from cold and can damp or excite the displacer for favourable movement.

This paper captures the work done in theoretically modelling and simulating the operation of a prototype FPSE from fundamental thermo-fluid dynamic principles. The first section of the paper describes the theoretical modelling of the prototype, by discretising the engine into a network of finite volume elements with representative finite difference equations. The second section discusses the design of the prototype engine that is currently being manufactured and the final section presents and discusses the simulation results of the prototype.

2. THEORETICAL MODELLING AND SIMULATION SETUP

A schematic representation of the prototype free piston Stirling engine is shown in Figure 1. The displacer shuffles the working fluid from the expansion space to the compression space and vice versa, in the respectively named compression and expansion strokes. A larger diameter was chosen for the displacer than the piston so as to shuffle a large amount of working fluid between expansion and compression spaces during a stroke. Heating is to be supplied by an electrical resistance pad, whereas cooling is to be supplied by a finned water jacket.

At the back of the piston is attached the piston magnet train, which together with the piston coil, forms the primary generator. The displacer shaft is located through the centre of the power piston and is attached to a smaller generator (motor) in the far back space. Flexure bearings (springs) attached to the respective displacer and piston provide a restoring force whilst minimising side forces. A coil spring attached to the displacer shaft in the back space stops the displacer from colliding with the container during the expansion stroke. The entire engine is sealed hermitically and pressurised with Helium as working fluid.
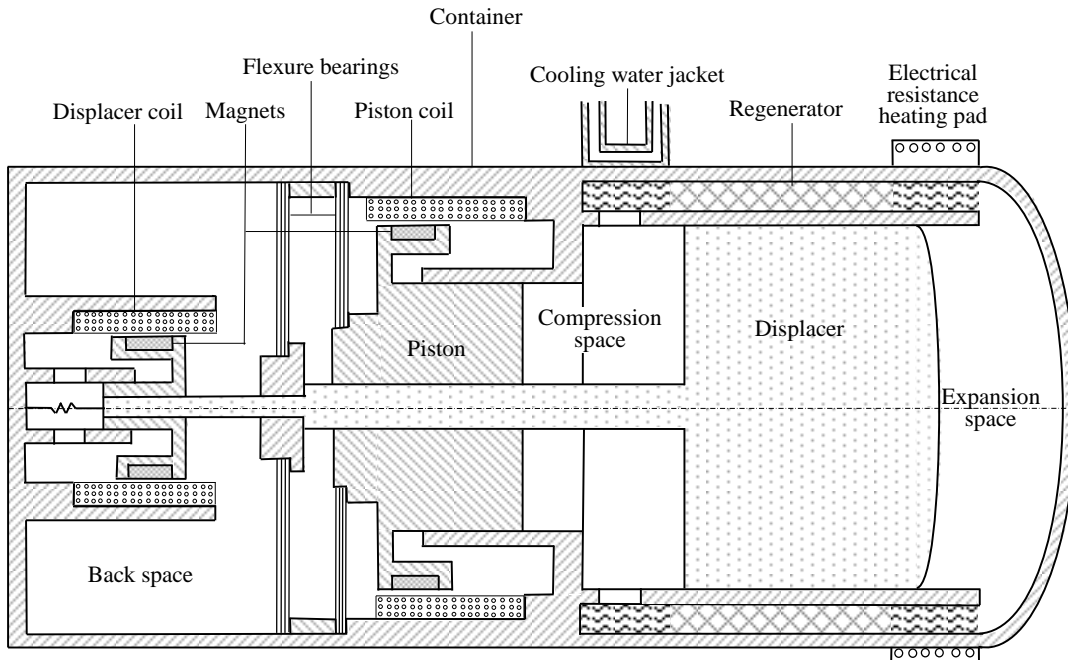

Figure 1: Schematic representation of the prototype free piston Stirling engine (FPSE).

2.1. Discretisation of the FPSE working space

The FPSE working space was discretised into a network of finite sized one-dimensional control volumes over which a system of finite difference equations was derived. Figure 2 shows the discretisation of the working space that was applied to theoretically simulate the

3

prototype. The heater, regenerator and cooler sections were each subdivided into 9 control volume elements, whereas the expansion, compression and back spaces were each modelled as a single adiabatic control volume with moving boundaries. It should be noted that control volumes 2 and N-1 are part of the respective heater and cooler sections, but for representation looks drawn out.
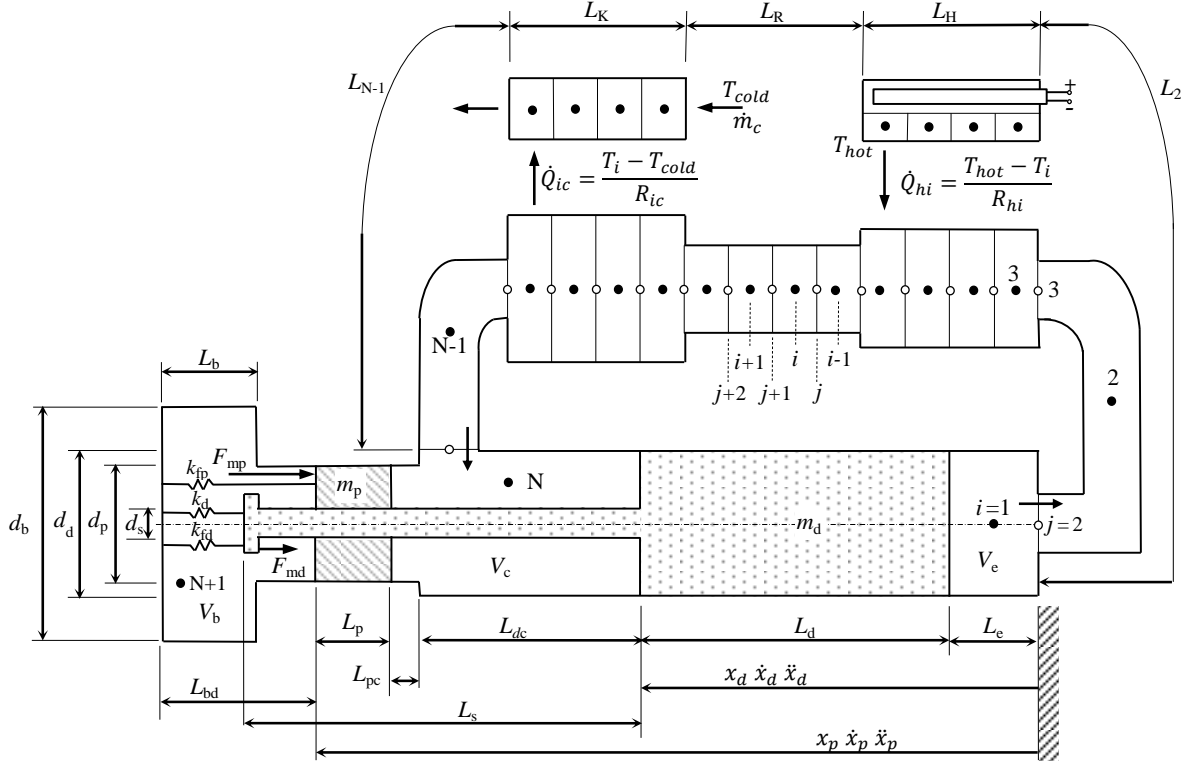
Figure 2: Discretisation scheme for the theoretical simulation of the prototype FPSE.

Control volumes, also called scalar elements or cells, were defined as containing a finite amount of mass with uniform thermodynamic properties such as pressure and temperature. The control volumes were numbered with subscript 'i' in the model with centres depicted by '●' in Figure 2. The conservation of mass and energy was applied to each control volume so as to solve the new mass and thermal energy (temperature) of the respective element with time. The model accommodates for different sized neighbouring control volumes, by utilising a so-called smallest face method where the pressure term only acts over the fluid-to-fluid contact interface.

At an interface or boundary between two consecutive control volumes, where convective transport occurs, was defined a so-called node. Nodes were numbered with subscript 'j' with centres depicted by '○', as shown in Figure 2. The function of a node is to define both the magnitude and direction of convective flow that results because of a working fluid pressure imbalance between neighbouring control volumes. A simple vector control volume was staggered-stacked over half the upstream and downstream control volumes as depicted in Figure 3 (b); to permit the solving of the momentum equation without the so-called *checkerboard* pressure phenomenon occurring [9].

For each control volume local Reynolds and Nusselt numbers were determined based on the flow velocity. This lead to local convective heat transfer coefficients for heat transfer between the working fluid and so-called "metal elements". A hydraulic diameter and effective heat transfer surface area was computed for the respective heating and cooling fins, and flat

plate heat transfer analogies were used to relate the flow Nusselt numbers to convective heat transfer coefficients. For the heater, heat transfer was modelled from the heating fins that were defined at constant hot temperature to the gas control volumes, and at the cooling side heat was rejected from the gas elements to the circulating cooling water. The channel of cooling water was subdivided into 9 elements so as to model the increase in cooling water temperature, as shown in Figure 2. For the regenerator section, heat transfer was modelled from the working fluid to 9 regenerator copper elements. The regenerator mesh heat transfer area was determined from its void fraction of 67% as outlined by Smith [10] and the convective heat transfer rate was related to the flow Stanton number as outlined by Kays and London [11] for one-dimensional flow.

Shown in Figure 3 (a) is the general discretised control volume i containing a finite amount of working fluid with the conservation of energy applied to it. The figure depicts the convective flow of mass and energy that enters and exits the control volume over cylindrical boundaries with areas A_j and A_{j+1} respectively. Also shown is the working fluid pressure force P_i acting over the fluid-to-fluid contact as well as energy generation by friction, the boundary work term $\dot{W}_b$ and the net convective heat transfer rate $\dot{Q}_{net}$. The conservation of momentum as applied to a staggered-stacked control volume at the generalised node j is shown in Figure 3 (b). Pressures and frictional forces from up- and downstream control volumes i were used to calculate the node velocity v_j.
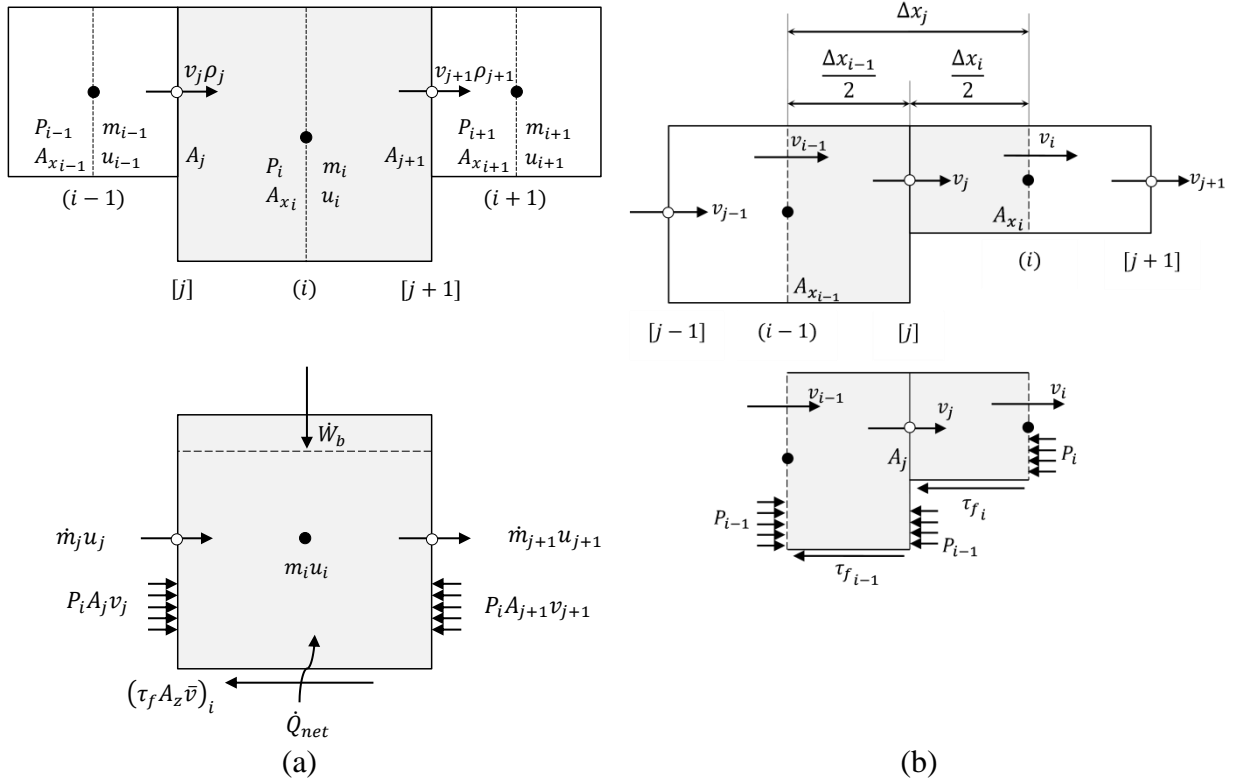
Figure 3: (a) Conservation of energy applied to a general control volume i .
(b) Conservation of momentum applied to a general interface node j .

5

2.2. Derivation of the governing system equations

The governing differential transport equations for the conservation of mass, momentum and thermal energy were derived as outlined by Bird et al. [12] for the working fluid. Spatial equation discretisation was accomplished by integrating the governing differential equations over cylindrical finite volume elements by use of Gauss's Divergence Theorem [13] to yield solvable finite difference equations. Eulerian integration was used to integrate the equations temporally to a fully-explicit form; to solve the control volume mass, momentum and thermal energy at a new time-step '$t + \Delta t$'.

The finite difference rate of change in mass m_i is written as

$$\frac{\Delta m_i}{\Delta t} = \rho_j v_j A_j - \rho_{j+1} v_{j+1} A_{j+1} \tag{1}$$

where the density ρ_j is obtained from upstream differencing, velocity v_j is determined from the momentum equation and the smallest fluid-to-fluid face area was used for A_j. The new control volume mass at a next time-step is given in its fully explicit form as

$$m_i^{t+\Delta t} = m_i^t + \Delta t \left(\rho_j v_j A_j - \rho_{j+1} v_{j+1} A_{j+1} \right)^t \tag{2}$$

The finite rate of change of momentum at an interface node is given by

$$\frac{\Delta}{\Delta t} \left(m_j v_j \right) = \left(\rho_{i-1} v_{i-1}^2 A_{xi-1} - \rho_i v_i^2 A_{xi} \right) + \left(P_{i-1} A_{xi-1} - P_i A_{xi} \right) - \left(\tau_{fi-1} \frac{A_{zi-1}}{2} + \tau_{fi} \frac{A_{zi}}{2} \right) \tag{3}$$

The mass m_j of the staggered vector element is taken as the sum of half the neighbouring control volume's mass, and the velocity v_i at the centre of the control volume is determined from a volumetric interpolation between neighbouring interface velocities v_j. Internal fluid stresses were modelled as a single frictional wall shear stress τ_f that acts to oppose fluid motion. The new node velocity at a next time-step is given by

$$v_j^{t+\Delta t} = \frac{\left(m_j v_j \right)^t + \Delta t \left(DM + DP + DF \right)^t}{m^{t+\Delta t}} \tag{4}$$

where DM, DP and DP represent the first, second and third terms of equation (3) respectively.

The finite rate of change in thermal energy is written as

$$\frac{\Delta}{\Delta t} \left(m_i u_i \right) = \left(\rho_j v_j A_j u_j - \rho_{j+1} v_{j+1} A_{j+1} u_{j+1} \right) + \dot{Q}_{net} + P_i \left(v_j A_j - v_{j+1} A_{j+1} \right) + \dot{W}_b + \tau_{fi} A_{z_i} \left| \overline{v}_i \right| \tag{5}$$

The internal energy u_j is obtained using an upwind differencing scheme. For simplicity in integrating the conservation of thermal energy equation to the model, boundary work has been decoupled from the reversible compression/expansion term and is represented by $\dot{W}_b$. Irreversible heat is generated by viscous dissipation and is modelled as surface friction, where the absolute velocity $\left| \overline{v}_i \right|$ is used to indicate the irreversible increase in thermal energy. The new total thermal energy at a next time-step is given by

$$\left(m_i u_i \right)^{t+\Delta t} = \left(m_i u_i \right)^t + \Delta t \left(DM_e + \dot{Q}_{net} + DP_e + \dot{W}_b + DF_e \right)^t \tag{6}$$

where DM_e, DP_e and DF_e represent the first, third and fourth terms of equation (5) respectively.

The equations of mass, momentum and energy are further linked by the working fluid pressure P_i that was obtained by applying the ideal gas law to each control volume, given by

$$P_i = \rho_i R_g T_i \qquad (7)$$

where temperature T_i was determined from the inertial energy and specific heat of the working fluid at constant volume C_v, given by

$$T_i = \frac{u_i}{C_v} \qquad (8)$$

2.3. Displacer and piston motion

As shown in Figure 4, the displacer and piston were both modelled as a finite sized rigid body that is subject to pressure, linear spring, electromagnetic and frictional forces. The displacer is depicted in Figure 4 (a) with the expansion space pressure P_e acting in the assumed positive direction (from right to left) and the compression space pressure P_c and back space pressure P_b acting in the negative direction. Frictional drag forces between the displacer body and wall τ_d and between displacer rod and piston τ_{dp} were modelled as flat plate fluid friction. The electromagnetic motor force acting on the displacer F_{md} is shown as acting against the positive displacer motion. However at the time of writing, the generator design parameters have not been fixed and therefore the electromagnetic load force was modelled as a pure linear damping force with damping coefficient c_p. The mechanical power generated is given by the product of piston load force and velocity.

(a)

(b)
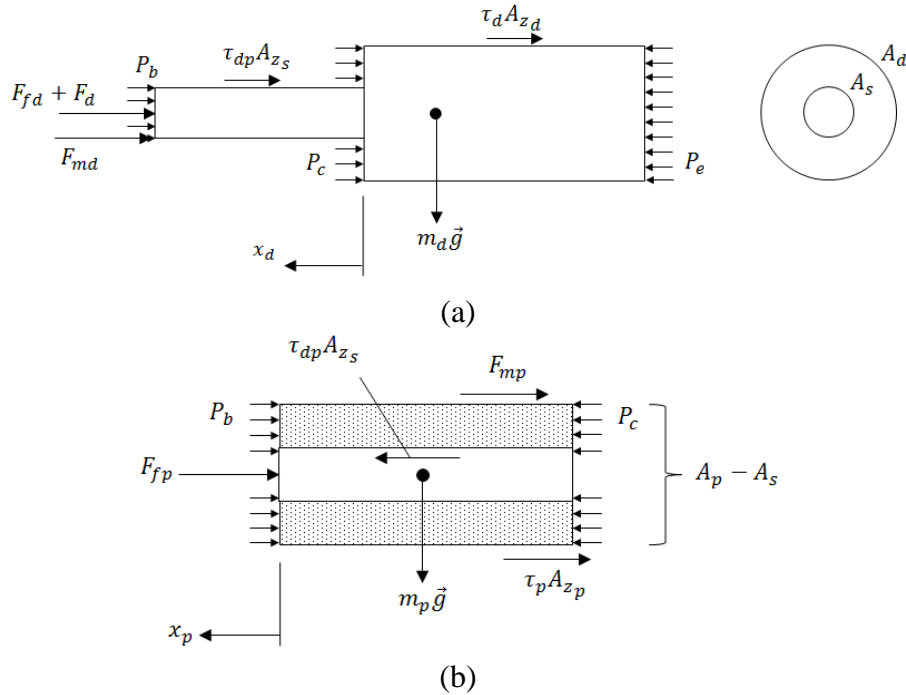
Figure 4: Free body diagrams for (a) Displacer, (b) Piston.

A schematic force diagram of the piston is depicted in Figure 4 (b) with the compression space pressure P_c and piston backspace pressure acting on its annular shaped body. The generator electromagnetic force F_{mp} is shown acting against the positive movement direction of the piston. In this case the engine is assumed to be mounted vertically with the displacer above the piston and the vector force of gravity acts in the assumed positive direction of movement.

Flexure springs were attached to both displacer and piston to centre them about their initial positions x_{d_o} and x_{p_0} respectively by providing a restoring force. The flexure springs were treated as linear springs and were therefore modelled by Hooke's law. The displacer flexure force F_{fd} is shown acting against positive net displacement $\left(x_d - x_{d0}\right) > 0$. In a similar fashion F_{fp} represents the piston flexure force. A force balance applied to the respective displacer and piston in the positive x-direction, yields

$$\Sigma F_d = P_e A_d - P_c \left(A_d - A_s\right) - P_{bd} A_s - \left(F_{fd} + F_d\right) - F_{md} - \tau_{dp} A_{zd} - \tau_d A_{zd} + m_d \vec{g} \tag{9}$$

$$\Sigma F_p = \left(P_c - P_{bp}\right)\left(A_p - A_s\right) - F_{fp} - F_{mp} + \tau_{dp} A_{zs} - \tau_p A_{zs} + m_p \vec{g} \tag{10}$$

The displacer and piston force balance equations were applied in Newton's 2nd law of motion to yield the assumed constant time-step acceleration, which was then temporally integrated to the new displacer and piston velocities and displacements in a fully explicit method. The velocities of at the next-time step are given by

$$v_d^{t+\Delta t} = v_d^t + \Delta t \left(\frac{\Sigma F_d}{m_d}\right)^t \tag{11}$$

$$v_p^{t+\Delta t} = v_p^t + \Delta t \left(\frac{\Sigma F_p}{m_p}\right)^t \tag{12}$$

The displacer and piston positions at the next time-step are given by

$$x_d^{t+\Delta t} = x_d^t + \left(\Delta t\right) v_d^t + \frac{\left(\Delta t\right)^2}{2}\left(\frac{\Sigma F_d}{m_d}\right)^t \tag{13}$$

$$x_p^{t+\Delta t} = x_p^t + \left(\Delta t\right) v_p^t + \frac{\left(\Delta t\right)^2}{2}\left(\frac{\Sigma F_p}{m_p}\right)^t \tag{14}$$

2.4. Program setup

Transient simulation of the theoretical model was achieved by computing the next time-step variables of the governing equations sequentially for each control volume. The conservation equations were solved with a so-called 'sweeping' method from control volumes $1 \rightarrow N$, meaning each control volume could only influence it's neighbouring control volume once per time-step. Nano-scale time-steps were used to solve the conservation equations stably and capture the so-called pressure waves that oscillate bi-directionally though the system.

Initially the engine was simulated from a complete state of rest, with engine control volume temperatures matching that of its ambient surrounding. However it was observed that the metal element temperatures, especially that of the regenerator, requires long simulation times to reach equilibrium. This is due to the requirement of nano time-steps to solve the gas momentum equation stably. To decrease the simulation time, a linear temperature interpolation for the working fluid and metal temperatures through the regenerator was computed by using the hot and cold side temperatures as boundaries.

The simulation program was developed in the Fortran 95 computer language and compiled by open source GNU Fortran for Windows. The prototype engine was simulated with model input parameters listed in Table 1, but can easily be changed as an input to the program. A sampling rate of 200 Hz was used to write model variables to a text file, for post processing and graphing in MatLab.
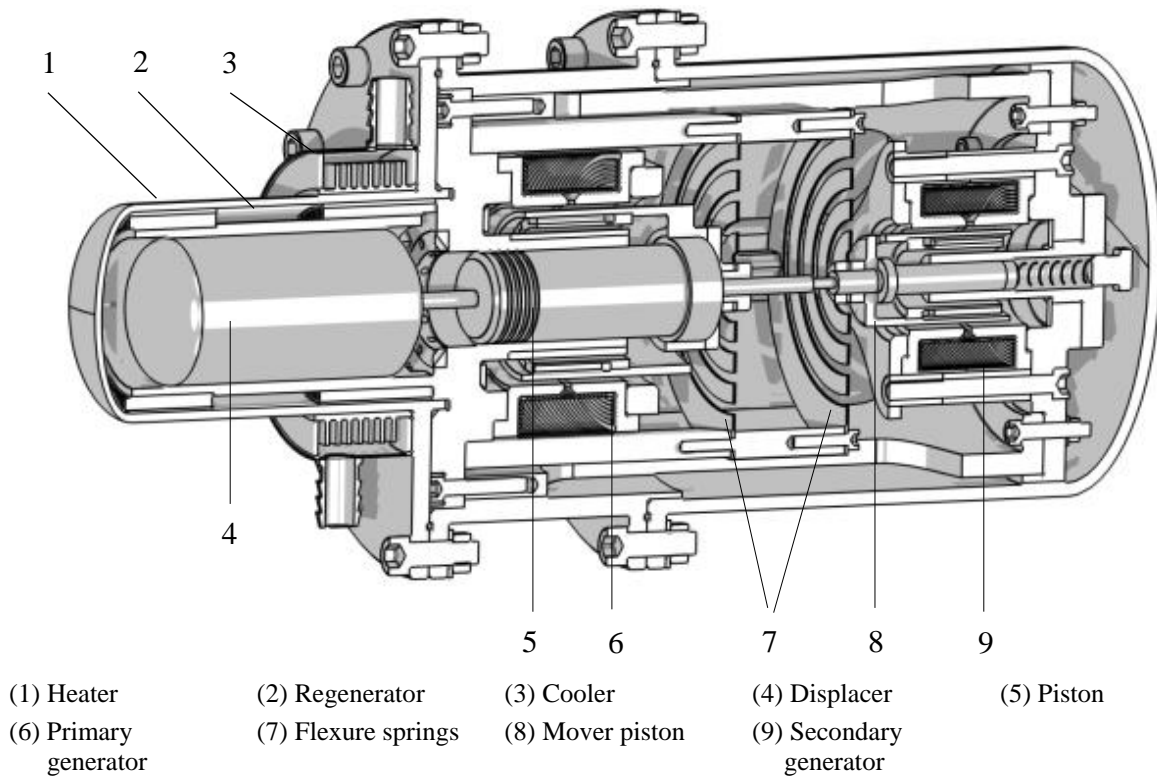
Table 1: Model input parameters.

Model parameters		
Time-step	5	$\times 10^{-9} \, s$
No. of heater elements	9	
No. of regenerator elements	9	
No. of cooler elements	9	
Operational parameters		
Initial charge pressure	3	MPa
Initial gas temperature	20	°C
T_{hot}	400	°C
T_{cold}	20	°C
Cooling water flow rate	0.1	ℓ / s
Generator load c_p	150	N.s / m
Design parameters		
Displacer mass	303	g
Piston mass	420	g
Displacer spring stiffness	6000	N / m
Piston spring stiffness	5000	N / m

3. DESIGN CONSIDERATIONS AND LAYOUT

The prototype engine under consideration is designed to be modular for testability; the generator magnet trains are completely interchangeable for stronger ones, the mover section can be removed from the engine chassis to make the engine more compact and the displacer and piston are both hollow to allow for a weight increase. An assembly drawing of the prototype under development is shown in Figure 5, with respective components discussed briefly in the section to follow.

3.1. Heater and cooler

The heater and cooler insides are finned tube heat exchangers with 90 fins each, to achieve high heat transfer rates between the working fluid and the metal section with a small pressure drop. Experimental heating is to be supplied by electric resistance wires, wound externally around the hot side, shown in Figure 5 (1). Cooling is to be supplied by a radially finned cooling jacket located over the cold side, as shown in Figure 5 (3).

(1) Heater	(2) Regenerator	(3) Cooler	(4) Displacer	(5) Piston
(6) Primary generator	(7) Flexure springs	(8) Mover piston	(9) Secondary generator	

Figure 5: Assembly drawing of the prototype engine under consideration.

3.2. Regenerator

The regenerator, shown in Figure 5 (2), consists of an annular tube staggered-stacked with copper mesh screens to form an overall void fraction of 67%. As hot gas flows from the heater to the cooler, heat is transferred from the gas to regenerator and "stored" to preheat the gas during the reverse flow cycle. This effectively precools the gas before it enters the compression space, and the reverse is true when the gas flows in the opposite direction. The regenerator functions to increase the efficiency of the engine, and its impact on engine performance will be determined experimentally when the prototype has been manufactured.

3.3. Displacer and piston

To achieve a high operating frequency the displacer, shown in Figure 5 (4), is to be as light-weight as possible whilst retaining sufficient structural integrity at high operating temperatures. Ideally it is envisaged to manufacture a displacer from aerospace grade titanium that is cobalt plated for wear resistance. Titanium has the unique properties of being extremely light weight, strong and durable and has high melting temperatures with very little thermal expansion. However, because titanium is very expensive and costly to machine, for a prototype the displacer was manufactured from tempered Aluminium 6 series that weighs twice as heavy. To compensate for the heavy displacer, the flexure springs attached to the displacer was made stiffer than that of the piston. The displacer diameter was machined smaller than that of the tube in which it is running so as to compensate for thermal expansion. Because of aluminium's lower melting temperature, the hot side temperature was limited to 400 °C.

The power piston, shown in Figure 5 (5), was designed to have more inertia (mass) than the displacer. This is to have the displacer lag out of phase behind the displacer movement, but also to desensitise the piston to spiking Lorentz electromagnetic forces. During the time of design, the optimal weight of the piston was unsure, therefore the piston was designed hollow and allow for weight increases during testing. Phosphor bronze was chosen as a good piston material because it's self-lubricating and has a high melting temperature.

3.4. Electric generator

As shown in Figure 5 (6) the primary generator consists of two soft steel cores with copper magnet-wire coils clamped in between. At the back of the piston is attached a magnet train that contains 12 Neodymium-Ferrite-Boron (NeFeB) grade 42 bar magnets. Movement of the so-called piston train through the core induces a change in magnetic flux through the core and leads to a change in flux linkage through the generator coils, ultimately producing an electric current.

The secondary generator was designed similarly, but was attached to the displacer rod and is located to the far right of the engine, as shown in Figure 5 (9). The addition of a secondary generator that can act either as an alternator or motor allows for direct displacer control. A feedback control system to control the displacer movement is yet to be designed.

3.5. Flexure springs

Flexure springs shown in Figure 5 (7) were modelled and designed as helical flat springs in the FEM environment. Different spring profiles were manufactured from stainless steel spring plate and are interchangeable and stackable in the modular design.

4. SIMULATION RESULTS AND DISCUSSION

Figure 6 shows the theoretically simulated results for the operating parameters given in Table 1. As shown in Figure 6 (a) the piston has a smaller stroke length than that of the displacer, because it is actively being damped by the primary generator. As seen the displacer leads the piston by 40.7° in a shared natural frequency of 25 Hertz. The power extracted from the piston in the primary generator is depicted in Figure 6 (d), where the peak power output matches the maximum piston velocity that occurs during the expansion stroke. Because an idealised generator was modelled with a constant damping coefficient, the damping force exerted on the piston in the simulation is directly proportional to the piston velocity, and the power extracted to the velocity squared. When the displacer reaches its maximum displacement of 14.2 mm it collides with the container and is brought to a sudden stand still. This is visually noticeable from Figure 6 (a) by the sharp trough shape on the displacer curve. Displacer collision also occurs when it reaches the minimum displacement of -14.2 mm, but more gently. The working space pressure depicted by Figure 6 (b) reaches its maximum pressure when all the working fluid has been displaced to the hot side, and the back space pressure peaks when the piston reaches its maximum displacement. Figure 6 (c) depicts the working space gas volumes for the compression and expansion spaces as well as the total volume of the working space fluid. The expansion and compression space volumes are about 90 ° out of phase, indicating that the displacer is primarily responsible for changing the working space volumes.
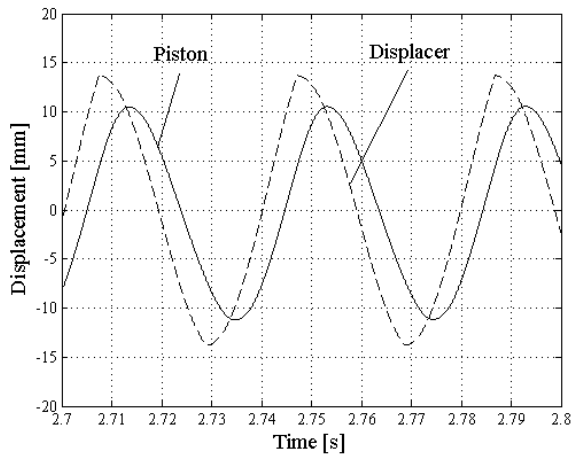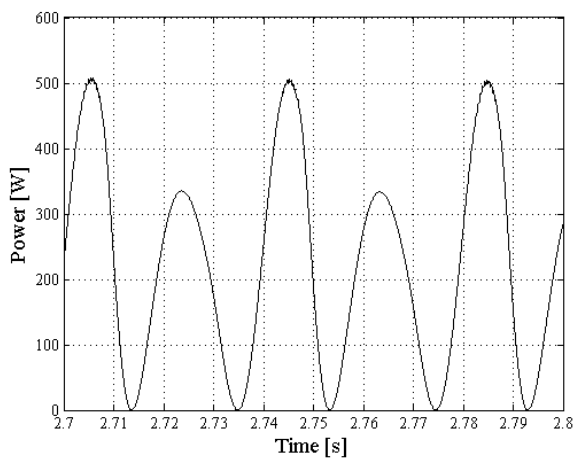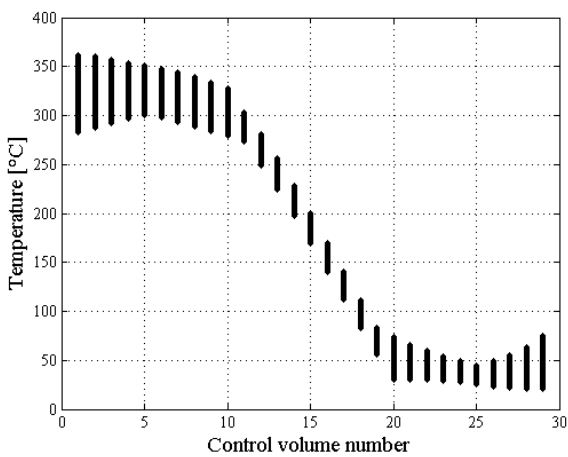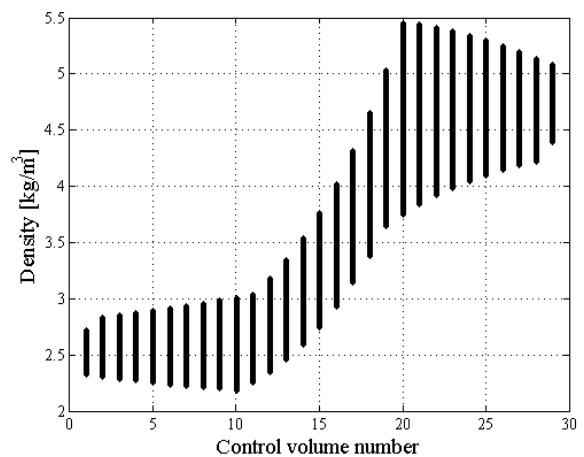
(a)
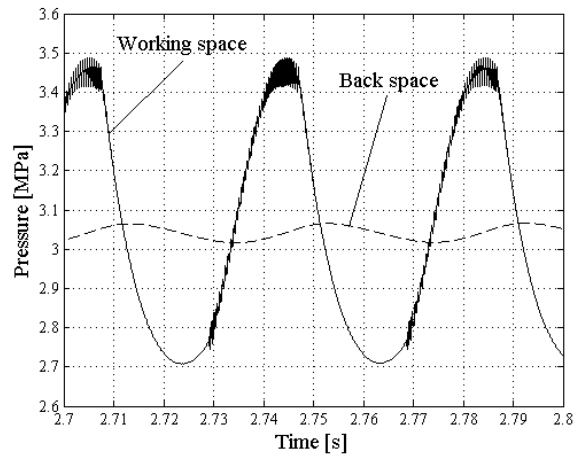
(b)
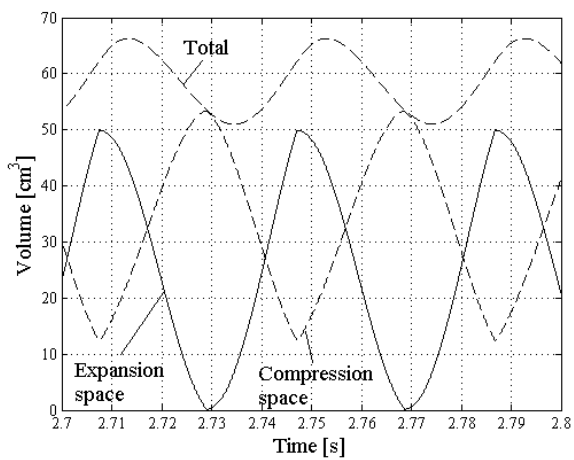
(c)

(d)

Figure 6: (a) Displacer and piston displacement. (b) Working- and back space pressures. (c) Working space volumes. (d) Primary generator output power.

The temperature and density of the working fluid for each control volume was also investigated and is depicted in Figure 7.


(a)

(b)

Figure 7: (a) Working fluid temperature and (b) density for each control volume.

Figure 7 (a) shows the range of the working fluid temperatures for each control volume and Figure 7 (b) the range of working fluid densities. Temperatures are hotter on the expansion space side with a lower gas density and vice versa on the compression space side. A linear temperature and density distribution exists between the hot and the cold side (through the regenerator), as expected.

To investigate the linkage of pressure and velocity terms in solving of momentum equation, the pressure and interface volumetric flow rate of each of the 30 control volumes that constitute to the working space are shown in Figure 8.
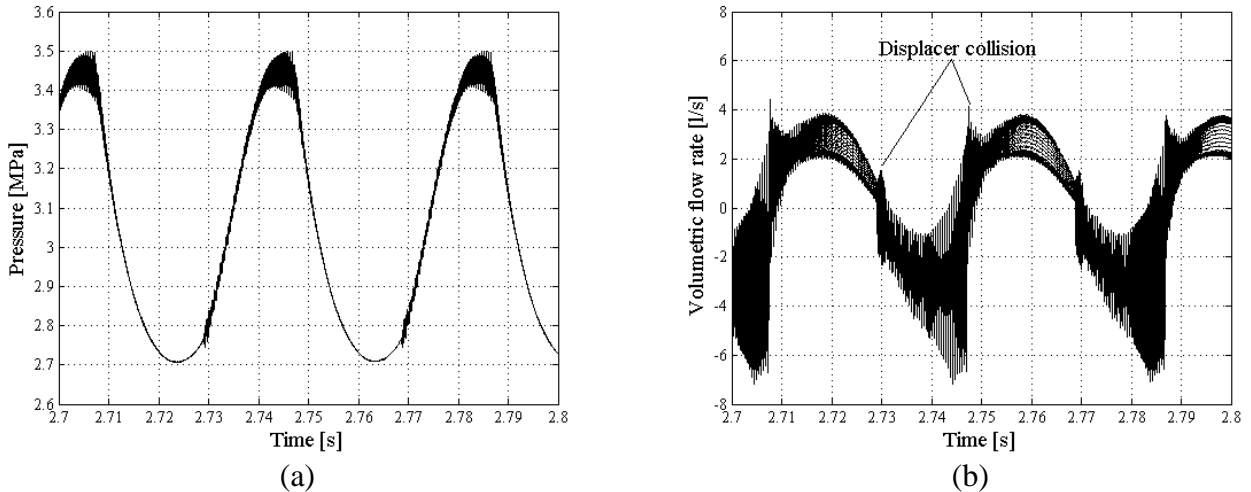
Figure 8: (a) Working fluid pressure and (b) interface volumetric flow rate distribution.

As seen in Figure 8 (a) the modelled frictional pressure drop at any time through the system is negligibly small when compared to the average charge pressure. The respective elemental pressures are very close to each other and can only be distinguished visually by zooming in on the figure. The working fluid pressure oscillates where it peaks at $3.5\,\text{MPa}$ as the piston and displacer first slows down and then starts moving in the opposite direction. As shown by Figure 8 (b) the oscillatory nature of the volumetric flow occurring at control volume interfaces is visually noticeable and ranges in a sinusoidal-like fashion between $-7\,\ell/\text{s}$ and $4\,\ell/\text{s}$. The negative volumetric flow rate is highly oscillatory and is linked to the region in which the pressure oscillates. A sudden spike or 'jump' in volumetric flow rate is noticed when the displacer collides with the container. The momentum of the moving displacer boundary is instantly dissipated, but the momentum of the adjacent gas control volume is not, introducing a so-called 'shock' on the momentum equation.

It can be shown that noticeable pressure and volumetric flow rate oscillation starts to occur when the direction of working fluid flow turns negative. Figure 9 depicts a zoomed-in view of (a) the control volume pressures and (b) volumetric flow rates over a time-window when the displacer reaches its maximum compression stroke and gently collides with the container. The displacer collision starts the oscillation that propagates through the system that evolves into a sinusoidal-like pressure wave, travelling between the compression and expansion space at the speed of sound in the working fluid. Modelling information about pressure travels against the default 'sweeping' direction of solver from element $N \rightarrow 1$. This results in numerical oscillation to occur as the momentum equation is less sensitive to information travel in this direction.

13
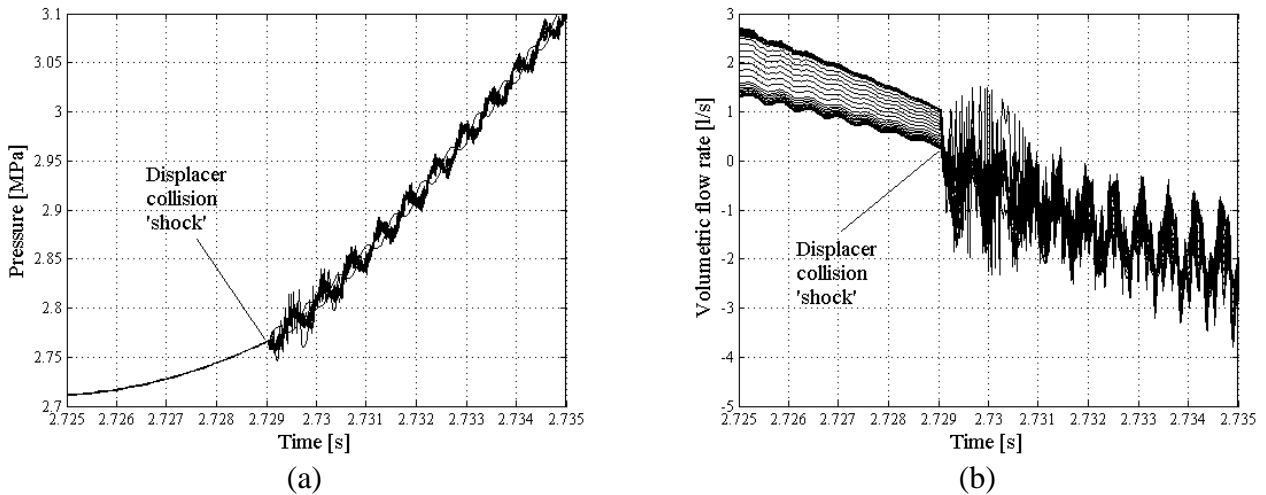
Figure 9: (a) Zoomed-in control volume pressures and (b) accompanying interface volumetric flow rates when oscillation starts.

Figure 10 depicts a zoomed-in view of (a) the pressure and (b) accompanying volumetric flow rate instants before displacer collision occurs for the expansion stroke. The pressure and volumetric flow rate waves have evolved from the erratic behaviour shown in Figure 9 into a steady sinusoidal-like wave, still displacing working fluid against the default sweeping direction of the solver.
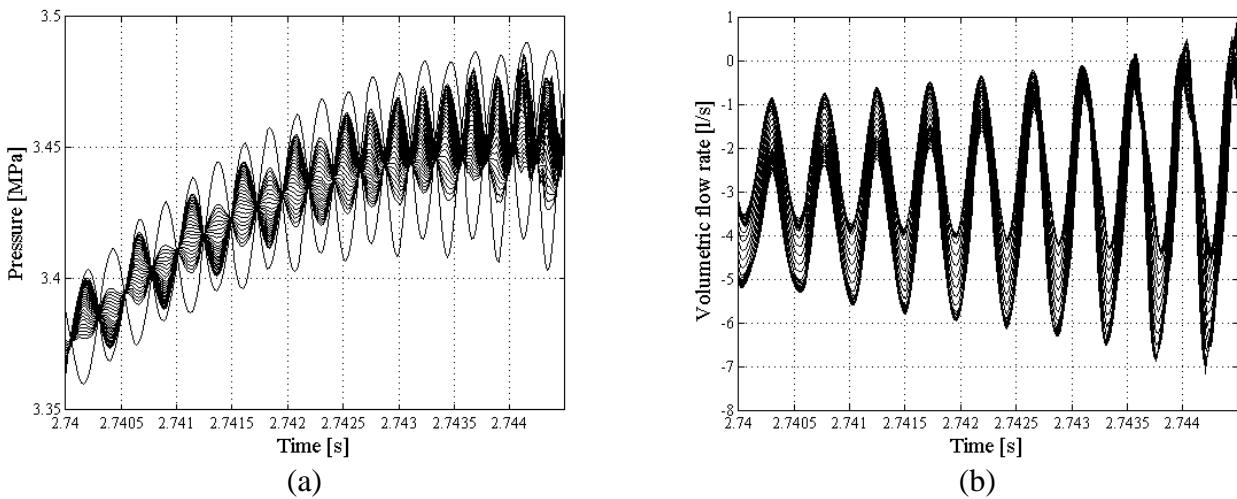
Figure 10: (a) Zoomed-in control volume pressures and (b) accompanying interface volumetric flow rates during expansion stroke.

14

A summary of the prototype simulation results is listed in Table 2. Although a peak power of 500 W was generated, the average generated power was only 240 W when averaged over the wave period. This was only achieved for an ideally modelled generator that is capable of extracting power that is directly proportional to the square of the piston velocity. For the simulation, the displacer proved to be reactive to the change in working space pressure and therefore it was not necessary for the motor to influence the displacer movement.

<p style="text-align:center">Table 2: Summary of model results</p>

Summarised results		
Average generated power	240	W
Peak power	500	W
Frequency	25	Hz
Phase difference	40.7	°
Peak pressure	3.5	MPa
Minimum pressure	2.7	MPa

5. CONCLUSIONS AND RECOMMENDATIONS

The study was aimed at modelling and simulating a FPSE prototype from fundamental thermodynamic theory so as to gain insight into the working mechanism of the engine. A theoretical model of a FPSE was derived by discretising the working fluid into a network of one-dimensional control volumes. The conservation of mass, momentum and energy was applied to each control volume so as to generate a system of finite difference equations, which was then solved with a fully-explicit time-bound method. The design layout of a modular and testable prototype that is under development was discussed and simulated in a Fortran 95 computer program. Simulation results showed that the prototype is capable of producing at least 200 W_e power from a lower temperature heat source under a charge pressure of 3 MPa with helium as working fluid. In the simulation the displacer was reactive to the change in working pressure and it was therefore not necessary to employ its attached motor.

The simulation showed that a fully-explicit method may be used to solve the conservation equations, given that nano-scale time-steps are used to effectively capture the pressure waves that oscillate bi-directionally through the working fluid. The momentum equation is prone to numerical instability especially when information travels against the default sweeping direction of the solver, from elements $N \rightarrow 1$. This is the disadvantage of a fully-explicit method and was outweighed by the ease and simplicity in which system equations could be transformed into a solution algorithm.

To decrease numerical oscillation it is recommended that the program be extended to a dual-sweeping solver, that is, every other time-step the conservation equations are solved from elements $N \rightarrow 1$. A more complicated model of the generator needs to be developed, that takes into account the actual change in flux linkage through the generator and the resulting electromagnetic force exerted by the coil. The manufacture of the prototype is currently underway and the validation of the model is planned for the near future. Ultimately it is envisaged that this work will pave the way towards the development of CHP Stirling systems in Southern Africa.

REFERENCES

[1] W. Beale, F. L. Heltsley, M. F. Feeney, R. C. Wagman, F. E. Woodling, and N. L.-Street, "Understanding Stirling Engines," *Volunt. Tech. Assist.*, no. 703, 1800.

[2] H. Karabulut, "Dynamic analysis of a free piston Stirling engine working with closed and open thermodynamic cycles," *Renew. Energy*, vol. 36, pp. 1704–1709, 2011.

[3] G. Prinsloo, A. Brent, A. Mammoli, and R. T. Dobson, "Modelling and Control Synthesis of a Micro-Combined Cooling Heat and Power Interface for a Concentrating Solar Power System in Off-grid Rural Power Applications," in *Concentrating Solar Power and Chemical Energy Systems (SolarPaces 2015)*, 2015.

[4] "Trinum - Solar Thermal Systems - Stirling Engine | Innova." [Online]. Available: http://www.innova.co.it/eng/catalog/products/trinum.html. [Accessed: 09-May-2016].

[5] I. N. Deetlefs, "Design, simulation, manufacture and testing of a free-piston Stirling engine," University of Stellenbosch, 2014.

[6] "Microgen Engine Corporation." [Online]. Available: http://www.microgen-engine.com/. [Accessed: 01-Jun-2016].

[7] "Twinbird Free Piston Stirling Cooler." [Online]. Available: http://fpsc.twinbird.jp/legacy/en/. [Accessed: 01-Jun-2016].

[8] J. M. Strauss, "Direct Piston Displacement Control of free-piston Stirling Engines," University of Stellenbosch, 2013.

[9] S. Patankar, "Numerical heat transfer and fluid flow," in *Series in coputational methods in mechanics and thermal sciences*, 1980, pp. 1–197.

[10] G. R. Smith, "Building, testing and modelling of a pulse tube cryogenic cooler," University of Stellenbosch, 2006.

[11] W. M. Kays and A. L. London, *Compact Heat Exchangers*, 3rd ed. New York: McGraw-Hill, 1984.

[12] R. B. Bird, W. E. Stewart, and E. N. Lightfoot, *Transport Phenomena*, Second. John Wiley & Sons, Inc., 2002.

[13] H. K. Versteeg and W. Malalasekera, *An Introduction to Computational Fluid Fynamics: The Finite Volume Method*, 2nd ed. Harlow: Pearson, 2007.

NOMENCLATURE

A = area (m^2)

a = acceleration (m/s^2)

d = diameter (m)

c_p = piston damping constant (N.s/m)

c_v = constant volume specific heat (J/kg.K)

F = force (N)

Subscripts

b = back space

bd = back space-to-displacer

c = compression space

$cold$ = cold side

d = displacer

F_d = back space spring force (N)

g = gravity (m/s^2)

k = spring stiffness (N/m)

L = lengths (m)

m = mass (kg)

N = last control volume number

Nu = Nusselt number

P = pressure (N/m^2)

Re = Reynolds number

R_g = helium specific gas constant

T = temperature (°C)

t = time (s)

u = specific internal thermal energy (J/kg)

V = volume (m^3)

v = velocity (m/s)

x = position (m)

$\dot{Q}$ = heat transfer rate (J/s)

$\dot{W}_b$ = rate of boundary work (J/s)

ρ = density (kg/m^3)

τ = shear stress (N/m^2)

$\dot{m}$ = mass flow rate (kg/s)

$\dot{x}$ = velocity (m/s)

$\ddot{x}$ = acceleration (m/s^2)

dc = displacer-to-compression space

dp = displacer-to-piston

e = expansion space

f = surface friction

fd = flexure spring, displacer

fp = flexure spring, piston

H = heater

hot = hot side

i = i-th control volume numbering

j = j-th node numbering

K = cooler

md = electromagnetic, displacer

mp = electromagnetic, piston

p = piston

pc = piston-to-compression space

R = regenerator

s = displacer shaft

x = cross sectional face area

z = perimeter contact area